Journal of Industrial and Engineering Chemistry 33 (2016) 209–220

Contents lists available at ScienceDirect

Journal of Industrial and Engineering Chemistry

journal homepage: www.elsevier.com/locate/jiec

Deep HOMO polymers comprising anthracene units for bulk heterojunction solar cells

Hyo Yeol Kim, Min Hee Choi, Yong Woon Han, Doo Kyung Moon *, Jung Rim Haw *

Department of Materials Chemistry and Engineering, Konkuk University, 1 Hwayang-dong, Gwangjin-gu, Seoul 143-701, Republic of Korea

ARTICLE INFO

Article history:
Received 24 July 2015
Received in revised form 3 October 2015
Accepted 3 October 2015
Available online 30 October 2015

Keywords:
Anthracene
Benzooxadiazole
Benzothiadiazole
Side chain manipulation
Bulk heterojunction polymer solar cells

ABSTRACT

Four anthracene-based D–π–A polymers, poly[anthracene-*alt*-4,7-bis(thiophen-2-yl)-5,6-bis(octyloxy)benzo[*c*][1,2,5]thiadiazole] (P1, P3) and Poly[anthracene-*alt*-4,7-bis(thiophen-2-yl)-5,6-bis(octyloxy)benzo[*c*][1,2,5]oxadiazole] (P2, P4), were successfully polymerized through Suzuki coupling reaction. The polymers include benzooxaediazole (BO), PAnoBO, and PAnoBO-EH exhibited the deep HOMO level (−5.39 eV or lower) because BO has a lower lying oxidation potential than Benzothiadiazole (BT). BO acceptor enhanced the electron withdrawing property of the polymers, inducing long-wavelength absorption and 0.05–0.1 eV reduction in the band-gap. For solar cells using a PAnoBO:$PC_{71}BM$ (1:4, w/w), the resulting J_{sc}, Voc, FF, and PCE were 3.1 mA/cm^2, 0.74 V, 48.8%, and 1.2%, respectively.

Introduction

For several decades, polymer solar cells (PSCs) with a bulk heterojunction (BHJ) structure have received considerable attention. They have several advantages over traditional PV cells such as their low cost, low weight, applied over large surfaces and use a sustainable source of energy: sunlight. Therefore, many investigations into new organic semiconductors with superior photovoltaic properties have been carried out [1–4].

In general, the active layer of a high-efficiency PSC is composed of a blended bulk heterojunction (BHJ) configuration consisting of an electron-donor (conducting polymer) and an electron acceptor (a fullerene derivative) [5,6]. For BHJ solar cells, high efficiency can be achieved by designing and tuning the chemical and structural parameters of the donor polymer (e.g., the conjugated backbone and side chains). In particular, the donor–acceptor (D–A) concept has been widely used in the design of conjugated polymers that are used in PSCs [7,8]. Their molecular orbitals can be fine-tuned by a choice of donor and acceptor. The ideal conjugated polymer for PSCs must have both broad absorption and a high absorption coefficient in the visible and near-infrared regions. Moreover, it must have high hole mobility and suitable HOMO and LUMO energy levels. Also, to assemble the active layer, it should also be miscible with the fullerene component to generate the appropriate nano-structured film [9,10]. Recently, high efficiency has been achieved using a conjugated polymer formed of a backbone with alternating units of an electron-rich donor and an electron-deficient acceptor [11–14].

Various organic electronic devices have been built using anthracene-based polymers as the donor unit in D–A type polymers. In particular, for organic photovoltaics (OPVs), good charge transport properties have been achieved in these polymers because of the planarity and rigidity of anthracene. Furthermore, anthracene has a low HOMO energy level, resulting in a high open voltage current (V_{oc}). However, further optimization of its solubility is necessary to enable the use of solution processing [15,16]. In general, unsubstituted anthracene derivatives without side-chains are poorly soluble in organic solvents. Therefore, in this report, we describe out attempts to improve the solubility of the anthracene-copolymer by introducing bulky side chains at the 9- and 10-positions of anthracene. However, the introduction of side chains can reduce the charge transport properties and interrupt the intermolecular packing of the copolymer when formed into a thin film. Therefore, it is important to select an appropriate side chain and acceptor to synthesize a copolymer with both good solubility and good intermolecular packing [17,18]. Also, the donor unit of a D–A type polymer should be paired with acceptors that

* Corresponding authors. Tel.: +82 2 450 3499; fax: +82 2 2201 6447.
E-mail addresses: dkmoon@konkuk.ac.kr (D.K. Moon), jrhaw@konkuk.ac.kr (J.R. Haw).

http://dx.doi.org/10.1016/j.jiec.2015.10.010
1226-086X/

lower the energy of the polymer LUMO. Benzothiadiazole (BT) has been widely used in PSCs as a strong electron-withdrawing unit. It is an electron-acceptor and has a quinoid structure, and these features can reduce the band-gap while allowing the formation of coplanar polymers [19–23]. Using benzoxadiazole (BO), which is a structure analog of BT, forms a polymer with lower HOMO and LUMO energy levels. In addition, polymers contain BO are air-stable. Moreover, when the polymer is blended with fullerene, high open-circuit voltages are achieved. However, in the case of several polymers based on BO, their low solubility led to the formation of low molecular weight polymers with low power conversion efficiencies (PCEs). Later, Wei et al. reported that the introduction of the octyloxy chain at the 5- and 6-positions of BO could improve polymer solubility [24–31].

In this report, we synthesized four D–A-type polymers, labeled P1, P2, P3, and P4, based on anthracene derivatives containing acceptors with different electron-withdrawing properties. The optical and electrochemical properties of BT and BO polymers are also described. We concluded that the introduction of BO in polymers P2 and P4 was the cause of the strong and broad absorptions observed in the UV–vis spectra. Furthermore, lower molecular orbital energy levels were achieved, including a 0.05–0.1 eV reduction in the band-gap and lower HOMO energies; for example, −5.33 and −5.36 eV for P1 and P3 and −5.39 and −5.53 eV for P2 and P4, respectively. Therefore, greater PCE values were obtained using the BO-containing polymers as the active layer in a conventional PV cell; namely, PCE was 1.2% for P2:$PC_{71}BM$ (1:4, 0.5 wt %).

Results and discussion

Synthesis and characterization of the polymers

Scheme 1 illustrates the chemical structure and synthesis of the monomers and polymers. The anthracene derivatives, which act as donors, 2,6-bis(4,4,5,5-tetramethyl-1,3,2-dioxaborolan-2-yl)anthracene (D1) and 2,2′-(9,10-bis(2-ethylhexyloxy)-9,10-dihydroanthracene-2,6-diyl)bis(4,4,5,5-tetramethyl-1,3,2-dioxaborolane) (D2), which has a 2-ethylhexyloxy side chain at the 9- and 10-C positions of D1 (Scheme 1) were synthesized. Additionally, benzo-2,1,3-thiadiazole, 4,7-bis(5-bromothiophene-2-yl)-5,6-bis(octyloxy)-benzo-2,1,3-thiadiazole (A1), which is a benzo[*c*][1,2,5]oxadiazole derivative, and 4,7-bis(5-bromothiophen-2-yl)-5,6-bis(octyloxy)benzo[*c*][1,2,5]oxadiazole (A2) were prepared. Using these donors (D1 and D2) and acceptors (A1, A2), the D–A type polymers poly[2,6-anthracene-*alt*-4,7-bis(thiophen-2-yl)-5,6-bis(octyloxy)benzo[*c*][1,2,5]thiadiazole] (P1), poly[2,6-anthracene-*alt*-4,7-bis(thiophen-2-yl)-5,6-bis(octyloxy)benzo[*c*][1,2,5]oxadiazole] (P2), poly[9,10-bis(2-ethylhexyloxy)anthracene-*alt*-4,7-bis(thiophen-2-yl)-5,6-bis(octyloxy)benzo[*c*][1,2,5]thiadiazole] (P3), and poly[9,10-bis(2-ethylhexyloxy)anthracene-*alt*-4,7-bis(thiophen-2-yl)-5,6-bis(octyloxy)benzo[*c*][1,2,5]oxadiazole] (P4) were prepared by using the Suzuki coupling reaction. The polymerization reaction was performed in toluene in the presence of $Pd(0)(PPh_3)_4$ catalyst, 2 M aqueous potassium carbonate as the base, and Aliquat 336 as a surfactant for 48 h at 90–95 °C. After completion of the polymerization, an end-capping reaction was conducted by adding bromobenzene and phenylboronic acid and stirring the solution for 3 h. The obtained powders were re-precipitated in methanol and purified by Soxhlet extraction using methanol, acetone, chloroform, and *o*-dichlorobenzene, in that order. Finally, the *o*-dichlorobenzene fraction was re-precipitated in methanol. The obtained powders were dark purple solids. P1, P2, P3, and P4 had isolated yields of 29, 59, 82, and 59%, respectively. Polymer P1 had low solubility in *o*-dichlorobenzene and, even at elevated temperatures, only partially dissolved. In contrast, P2 was mostly soluble in *o*-dichlorobenzene. Both P3 and P4 showed good solubility in general organic solvents such as chloroform ($CHCl_3$), tetrahydrofuran (THF), chlorobenzene, and *o*-dichlorobenzene. The synthesized polymer structures were further analyzed by ^1H NMR and elemental analysis (EA) (see in ESI, Fig. S1).

Table 1 summarizes the molecular weights and thermal properties of the polymers. Number average molecular weights (M_n) were determined using gel permeation chromatography with polystyrene as the standard and were 15, 13, 21, and 23 kDa with narrow PDI distributions of 1.6, 1.5, 1.9, and 1.3 for polymers P1–P4, respectively. Using thermogravimetric analysis (TGA), P1–P4 we were shown to have high thermal stability, even between 250 and 290 °C where they showed 5 wt% loss. These results imply that the synthesized polymers could be used in polymeric solar cells or other optoelectronic devices, as shown in Fig. S2.

Optical properties

The UV–vis spectra of the polymers in the solution phase (Fig. 1(a)) and film-phase (Fig. 1(b)) are shown in Fig. 1, with a summary in Table 2.

As shown in Fig. 1, all polymers have two absorption peaks in the range of 300 to 800 nm. The absorption peaks that appear at high-energy wavelengths (ca. 349–356 nm) are due to π–π^* transitions. In contrast, the absorption peaks at lower energy wavelengths (ca. 505–548 nm) are due to the intramolecular charge transfer (ICT) between the donors and acceptors [32,33].

In solution (*o*-dichlorobenzene), polymers P1 and P2 have similar absorption peaks with pairs of peaks was observed at 349 and 541 nm for P1 and 350 and 548 nm for P2. On the other hand, in solution, P3 and P4, which both have a 2-ethylhexyloxy side chains, the absorption peaks were blue-shifted with respect to P1 and P2 at 348 and 505 nm for P3 and 356 and 507 nm for P4. The maximum absorption wavelengths of the thin films (λ_{max}) were red-shifted by 1–48 nm compared to the solution state UV–vis spectra. This implies that in the film state there are stronger intermolecular interactions between the polymer chains than the solution state, leading to efficient 2-D stacking [34]. In particular, for P1 and P2, the absorption peaks located at about 600 nm have shoulders that arise due to their ordered solid-state structures. This phenomenon indicates that the polymers not only effectively reduce the steric hindrance in the solid state, but they also promote stronger chain stacking, even in solution [35]. Moreover, in the film state, the polymers have λ_{max} at 363 and 596 nm for P2 and 357 nm and 547 nm for P4, and these values are red-shifted (Δ = 1–48 nm) compared to those of polymers P1 and P3. For BO-containing polymers, better absorption intensity at longer wavelengths was observed compared to the BT-containing polymers. This is due to the greater electronegativity of oxygen than sulfur, which increases ICT effect in BO-compared to BT-containing polymers [36]. The electron configuration of oxygen and sulfur are $1s^2/2s^2/2p^4$ and $1s^2/2s^2/2p^6/3s^2/3p^4$, respectively. The nucleus of oxygen can affect the neighboring electrons and exerts a large force on the peripheral electron because an oxygen atom is smaller than a sulfur atom [37]. The calculated band-gaps of P1–P4 were calculated from the UV onset values and are 1.91, 1.86, 1.93, and 1.83 eV, respectively. The BO-containing polymers P2 and P4 have smaller band-gaps than either P1 or P3 [26].

Orientation analysis

The spacer structure of the polymers and the ordering and crystallinity of the thin films were analyzed by X-ray diffraction at annealing temperatures.

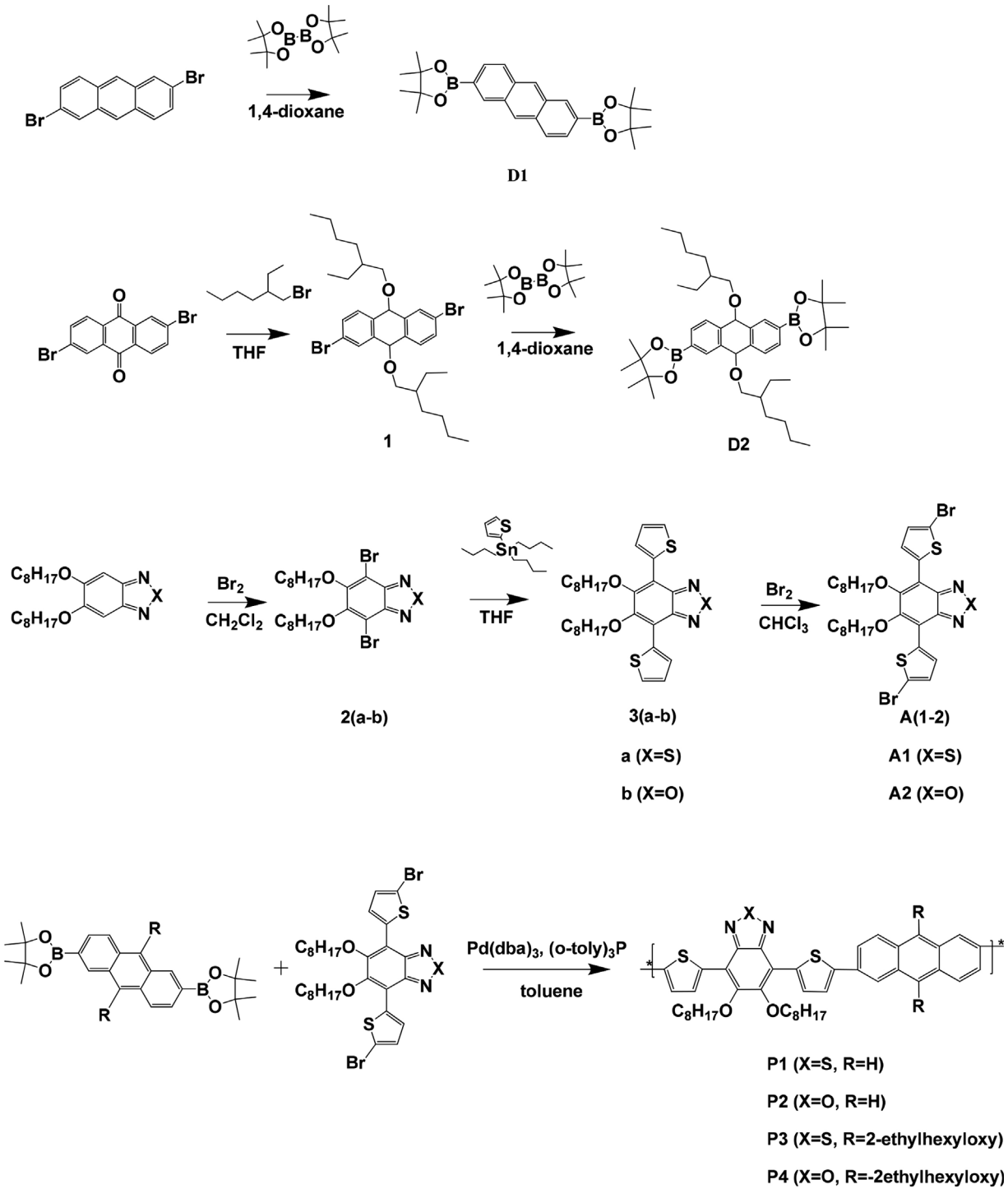

Scheme 1. Synthesis of monomers and polymers.

Table 1
Physical and thermal properties of polymers.

Polymer	Yield [%]	M_n [g/mol]	M_w [g/mol]	PDI	T_d [°C]
P1	29	15,000	24,000	1.6	280
P2	59	13,000	19,500	1.5	250
P3	82	21,000	41,000	1.9	275
P4	59	23,000	32,000	1.3	290

Determined by GPC in chloroform using polystyrene standards.

To analyze the ordered structure of the polymer, X-ray diffraction analysis of the polymer film was carried out in out-of-plane mode (Fig. 2(a)). For P3 and P4 films, sharp diffraction peaks (1 0 0) were observed at 5.28 and 5.04°, resulting from their (1 0 0) lamellar structures. The lamellar *d*-spacings (d_1) were calculated using Bragg's law ($\lambda = 2d\sin\theta$) and are 16.88 and 17.31 Å. In the case of P3 and P4, the (0 1 0) peak was not observed, which indicates the formation of an edge-on crystalline structure. P1 and P2 had reflections at 3.94 and 4.62°, respectively, due to the

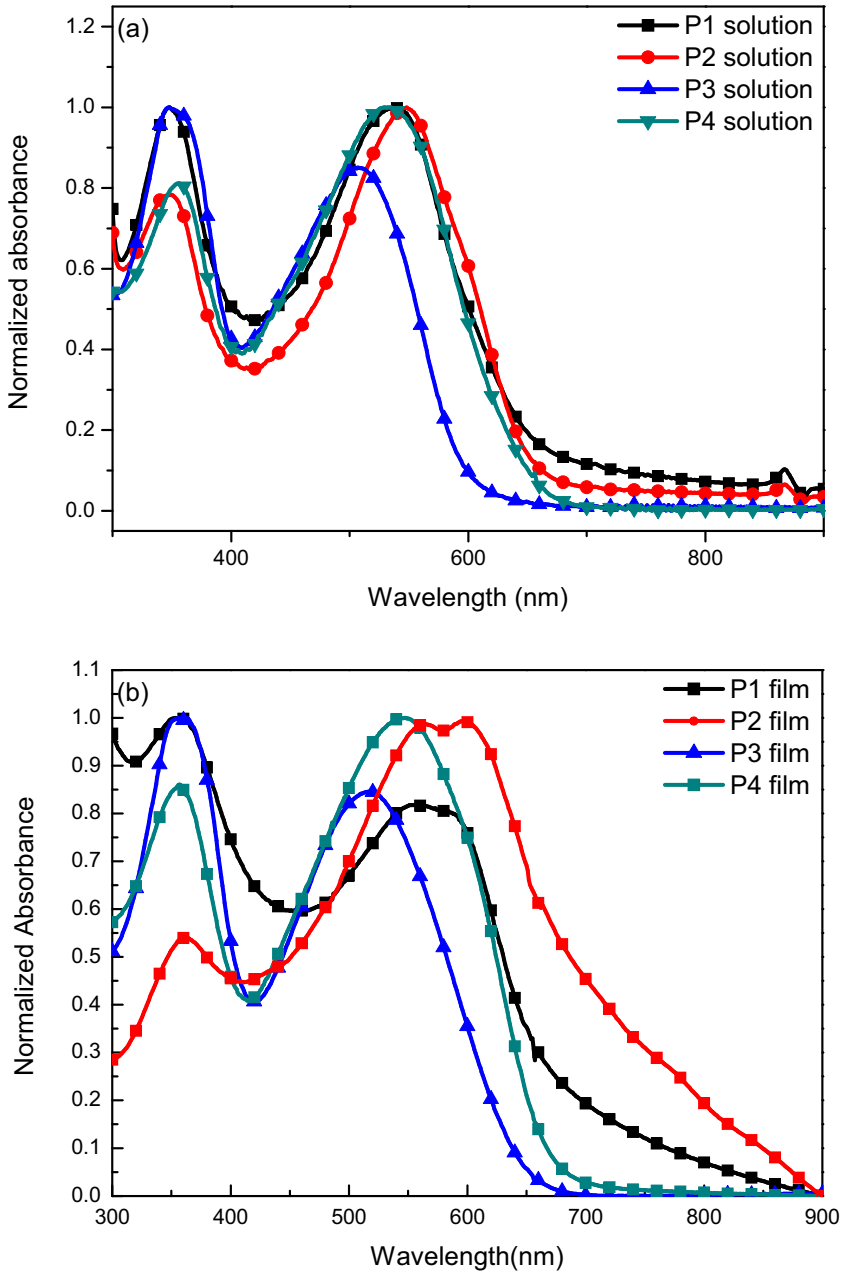

Fig. 1. UV–vis absorption spectra of polymers in solution (a) and film (b).

(*h* 0 0) lamellar structure. Similarly, the (0 *h* 0) lamellar structures in P1 and P2 gave rise to reflections at 21.79 and 21.55°, respectively. These observations indicate a bimodal crystal structure in an out-of-plane mode. Thus, using Bragg's law ($\lambda = 2d \times \sin\theta$), the highly ordered (1 0 0) lamellar *d*-spacings (d_1) are 22.43 and 19.12 Å. π–π stacking distances (d_π) are 4.08 and 4.12 Å. Due to the π–π stacking peak observed at the (0 1 0) face of the out-of-plane mode, we concluded that the crystal

Table 2
Optical and electrochemical data of all polymers.

Polymer	UV–vis absorption					
	ODCB sol	Film			Cyclic voltammetry	
	λ_{max} [nm]	λ_{max} [nm]	λ_{onset} [nm]	$E_g^{opt.a}$ [eV]	E^{ox}_{onset}/HOMO [*V*]/[eV]	LUMO[b] [eV]
P1	349, 541	353, 553, 583	649	1.91	1.00/−5.33	−3.42
P2	350, 548	363, 563, 596	667	1.86	1.07/−5.39	−3.53
P3	348, 505	356, 518	642	1.93	1.03/−5.36	−3.43
P4	356, 507	357, 547	678	1.83	1.20/−5.53	−3.70

[a] Calculated from the intersection of the tangent on the low energetic edge of the absorption spectrum with the baseline.
[b] LUMO = HOMO + E_g.

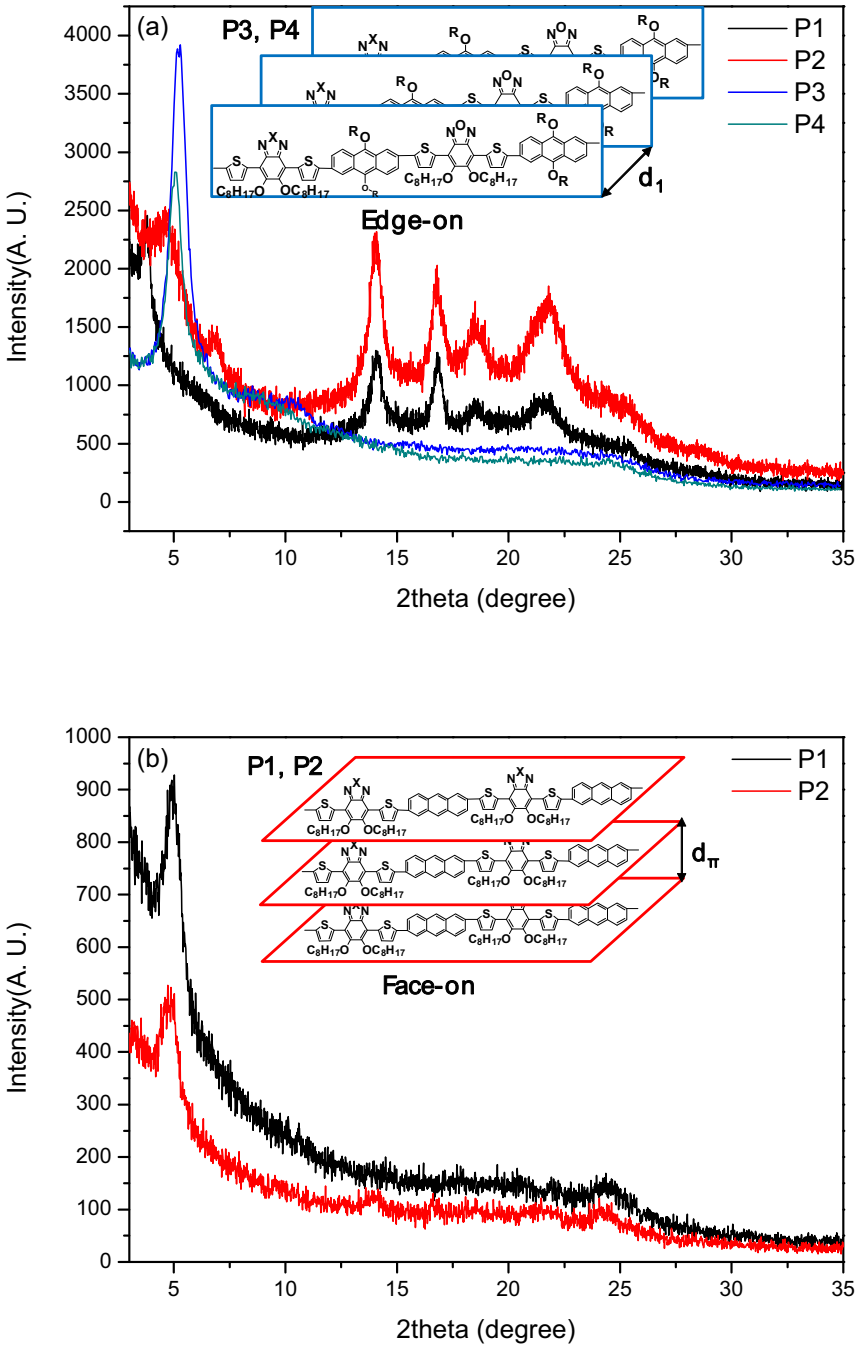

Fig. 2. X-ray direction pattern of polymers on a silicon wafer and a Polymer on silicon wafer out-of-plane (a) and in-plane (b) mode.

structure in the polymer film has a face-on orientation. This was confirmed by further analysis using in-plane mode X-ray diffraction. The in-plane mode X-ray diffraction analysis results are shown in Fig. 2(b) for P1 and P2 polymer films. At both low and high angles, crystalline peaks were observed for P1 and P2, with a predominance of low-angle sharp peaks. This result indicates the formation of a film with face-on rich mixed orientation. P1 and P2 polymers with the face-on structure have shoulder peak, and the λ_{max} values for P1 and P2 are 583 and 596 nm, respectively. The UV–vis spectra of the films, shown in Fig. 1(b), can be explained by ICT effect between the donors and acceptors.

Computational studies

To identify the electronic properties, molecular geometries and density of states distributions of the polymers, density functional theory (DFT) calculations were made. DFT calculations were performed using Gaussian 09 with the hybrid B3LYP correlation functional and the 6-31G(d) split-valence basis set. For computational simplification, the alkoxy side chains on both the BT and BO acceptor units were replaced by methoxy groups, and the branched alkyl side chains on the anthracene unit were replaced by *sec*-butyl groups. The polymer backbones were simplified to oligomers with one repeating unit for the calculation. The

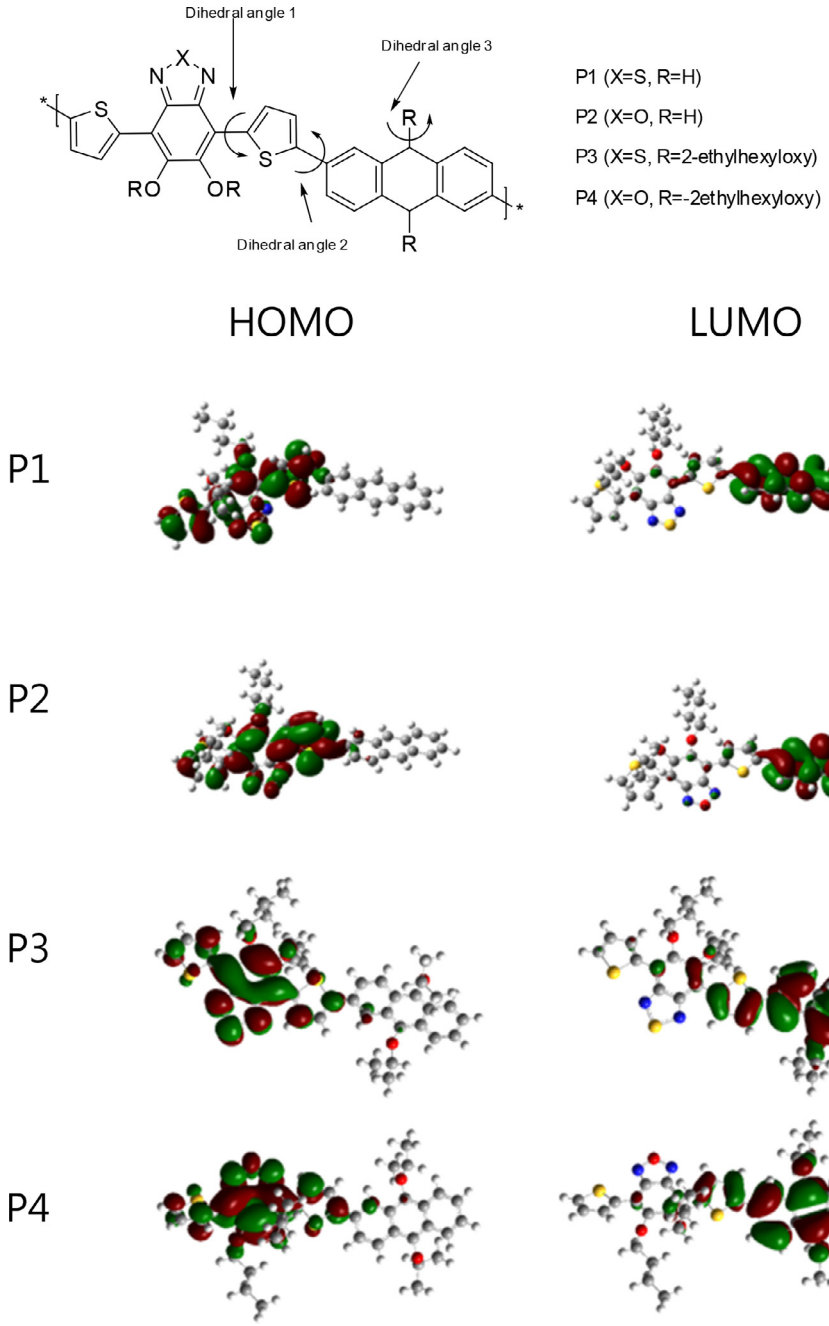

Fig. 3. Calculated HOMO, LUMO orbitals and dihedral angles position of polymers.

calculated HOMO and LUMO orbitals are shown in Fig. 3, and Table 3.

As shown in Fig. 3, the HOMO orbitals are localized on the donor anthracene moiety. In contrast, the LUMO orbitals are localized over the acceptor and spacer unit due to the non-bonding lone pair of the nitrogen atom and the quinoid structure generated between electron-withdrawing sulfur/oxygen atoms. The DFT calculations revealed that polymers P1–P4 have well-defined D–π–A structures and intramolecular charge transfer properties (i.e., the HOMO to LUMO transition is a donor to acceptor ICT effect) [38].

Fig. 3 shows three marked dihedral angles (1, 2, and 3) of the optimized polymer backbones (P1–P4) determined by DFT calculations. In all four polymers, dihedral angle 1 is similar, ranging from 8 to 10°. Polymers P1 and P2, which contain donor D1, have values of 23 and 27° for dihedral angle 2. In contrast, in polymers P3 and P4, which contain donor D2, dihedral angle 2 was larger (36°). This difference can be attributed to the additional side chains attached to the 9- and 10-C positions of anthracene, which increased steric hindrance between the backbone and side chain. Dihedral angle 3 is 76° for both P3 and P4.

Table 3
Calculated parameters.

Polymer	Dihedral angle (°)				
	1	2	3	$HOMO^{cal}$ [eV]	$LUMO^{cal}$ [eV]
P1	8	27	–	−4.23	−1.94
P2	10	23	–	−5.04	−2.23
P3	8	35	76	−6.68	−0.58
P4	9	35	76	−6.75	−0.53

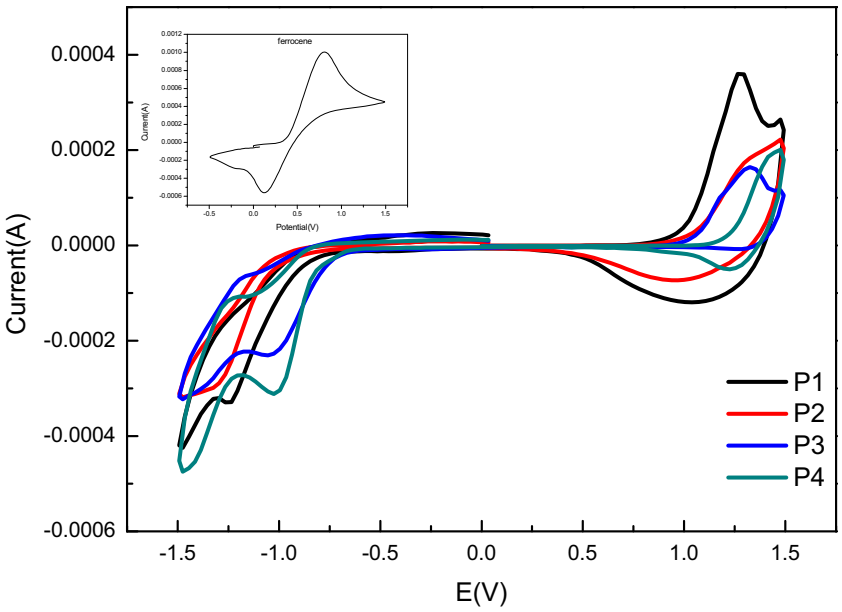

Fig. 4. Cyclic voltammograms of polymers.

These results agree with the UV–vis spectra of the films of P1 and P2; that is, the presence of shoulder peaks. Moreover, X-ray diffraction peak analysis showed that P1 and P2 with superior planarity display face-on structures; in contrast, P3 and P4 have edge-on structures. The DFT calculated HOMO energies for P1–P4 are −4.23, −5.04, −6.68, and −6.75 eV, respectively. These indicate that the HOMO energy is lowered as the electron donating properties of the donor segments increase. Indeed, You et al. showed that in a push-pull system, the HOMO energy is determined by the donor strength [8]. Thus, we confirmed that polymers containing D2 and BO had lower HOMO energy level than those containing either D1 or BT.

Electrochemical properties

Cyclic voltammograms (CV) of the polymer thin films were measured in acetonitrile solution using 0.1 M tetrabutylammonium-hexafluorophosphate (TBAHFP) in acetonitrile solution. As shown in Fig. 4, clear oxidation peaks were observed for all polymers, and these are due to their D–A structure. The oxidation onset values (E_{ox}^{onset}) for P1–P4 are 1.00, 1.07, 1.03, and 1.20 V, respectively. The corresponding calculated HOMO levels are −5.33, −5.39, −5.36, and −5.53 eV, respectively. Due to the higher oxidation stability of oxygen compared to sulfur, P2 and P4 have lower HOMO energies compared to P1 and P3. Therefore, higher V_{oc} are expected for devices containing P2 and P4. The above-mentioned optical band-gap and HOMO level difference allowed us to calculate the LUMO energies of P1–P4, which are −3.52, −3.67, −3.43, and −3.70 eV, respectively [39,40]. To have oxidation stability, the HOMO level should be lower than the air oxidation threshold (−5.27 eV). Thus, the low HOMO levels (≤−5.25 eV), indicates good oxidation stability.

Photovoltaic characteristics

To investigate the photovoltaic (PV) properties of the synthesized polymers, conventional BHJ PSCs were prepared. The photovoltaic properties of the polymers were assessed by preparing PSA devices with an ITO/PEDOT:PSS/polymer:$PC_{71}BM$/BaF_2/Ba/Al structure. All devices were prepared and encapsulated in a glove box. *J–V* characteristics were measured at ambient atmosphere with an active area of 4 mm^2. The weight ratio of polymer to $PC_{71}BM$ was varied, and samples with ratios of 1:2, 1:3, and 1:4 were prepared. *o*-Dichlorobenzene was used as the solvent. The *J–V* curves of the devices at the optimized weight ratios are shown in Fig. 5(a), and the corresponding IPCE curves are shown in Fig. 5(b). The PV properties of the prepared PSCs are summarized in Table 4. Even at elevated temperatures, P1 was only partially soluble in *o*-dichlorobenzene. Therefore, the solution could not be filtered through a PTFE filter, so we couldn't make P1 device. For polymer P2 at a weight ratio of 1:4, V_{oc}, short-circuit current (J_{sc}), fill factor (FF), and PCE were 0.74 V, 3.1 mA/cm^2, 48.8%, and 1.2%, respectively. For polymer P4, with a weight ratio of 1:2, V_{oc}, J_{sc}, FF, and PCE were 0.84 V, 3.8 mA/cm^2, 31.4%, and 1.0%, respectively. V_{oc} is determined by the difference between the HOMO of the polymer and the LUMO of $PC_{71}BM$. The obtained V_{oc} values from the prepared devices are in good agreement with the HOMO levels obtained from CV measurements and DFT calculations. P2 and P4, which contain BO and are stable to oxidation, have low HOMO energies and large V_{oc} values. Particularly, P4 has a higher J_{sc} compared to P2, which could be ascribed to the high quantum efficiency due to the edge-on structure of P4. However, due to its relatively large series resistance (R_S) and small shunt resistance (R_{SH}), P4 has lower FF than P2, and a PCE of only 1.0%, which is lower than that of P2 [41,3].

For polymer P3, with a weight ratio of 1:3, V_{oc}, J_{sc}, FF, and PCE were 0.64 V, 1.4 mA/cm^2, 25.2%, and 0.2%, respectively. Because BT is the acceptor in P3, the observed V_{oc} was ow compared to P2 and P4. Also, the FF and J_{sc} values are lower; consequently, the device efficiency was low. This can be explained by the series resistance (R_S) and shunt resistance (R_{SH}). At lower R_S and higher R_{SH}, there is a lower chance of recombination of excitons, which can improve the properties of the interface with the buffer layer [42]. However, in the case of P3, similar R_S and R_{SH} values were obtained, which induced high current loss and low J_{sc}.

Morphology analysis

The morphologies of polymer/$PC_{71}BM$ blend films were analyzed by AFM (Fig. 6). Similar RMS roughness values were

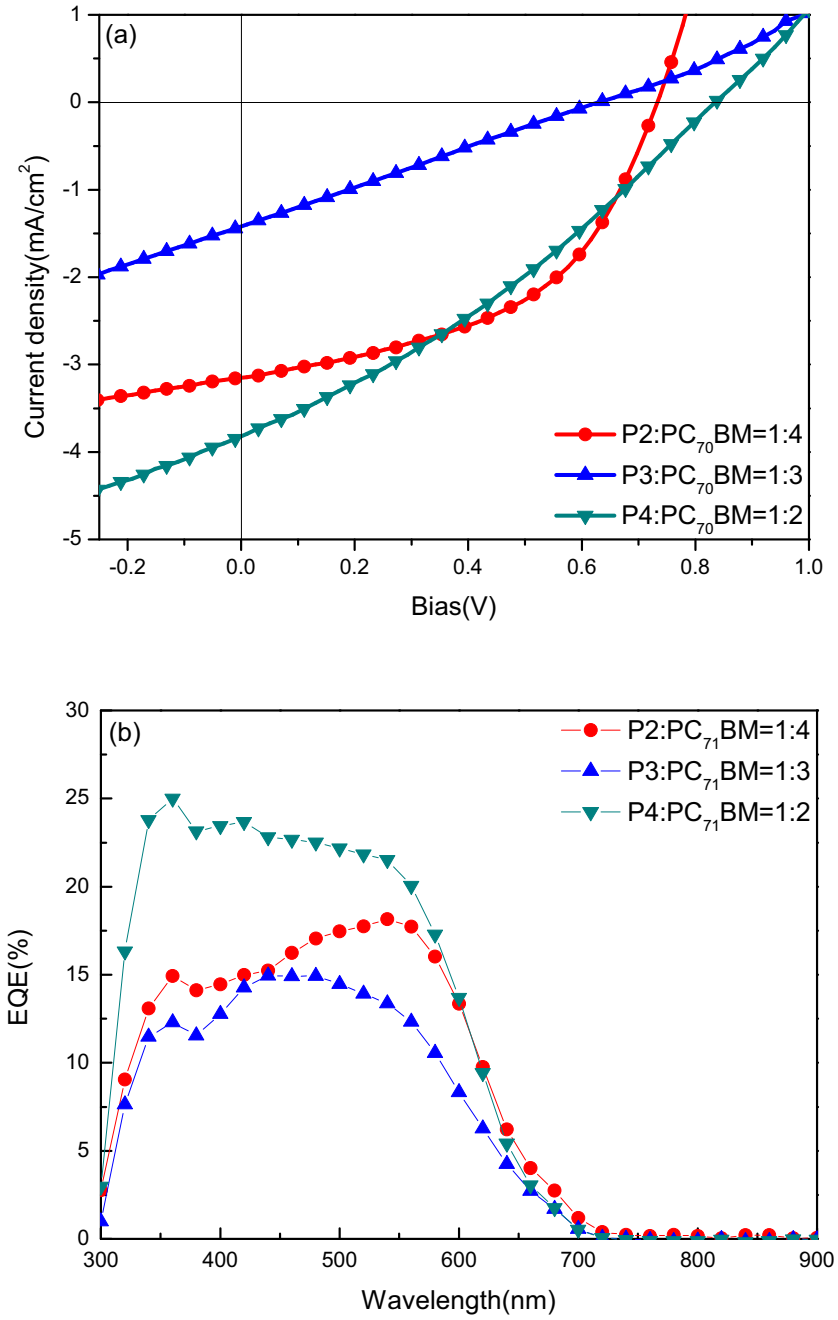

Fig. 5. *J–V* curves of PSCs with different polymer:$PC_{71}BM$ ratios under AM1.5G illumination, 100 mW/cm^2 (a) and The IPCE spectra of PSCs with different polymer:$PC_{71}BM$ ratios (b).

obtained for films of P2, P3 and P4 blended with $PC_{71}BM$ (0.49, 0.41, and 0.42 nm). In general, a smaller RMS value indicates a more homogeneous, smoother, surface; however, morphology is affected more by the surface state than by small deviations of RMS values [43]. Both P2/$PC_{71}BM$ and P4/$PC_{71}BM$ blends showed uniform nanostructures with good intermixing and phase separation to form percolation pathways. However, no phase separation was observed for P3 [44,45]. A consequence of these morphological factors is that the FF values for P2 and P4 were 48% and 31%, respectively, and both J_{sc} values were greater than 3 mA/cm^2.

Table 4
Photovoltaic properties of polymers.

Polymer	$PC_{71}BM$ ratios (w:w)	V_{OC} [V]	J_{SC} [mA/cm^2]	FF [%]	PCE [%]	R_S (Ω cm^2)	R_{SH} (Ω cm^2)
P1	–	–	–	–	–	–	–
P2	1:4	0.737	3.1	48.8	1.2	60	1111
P3	1:3	0.636	1.4	25.2	0.23	481	470
P4	1:2	0.838	3.8	31.4	1.0	168	448

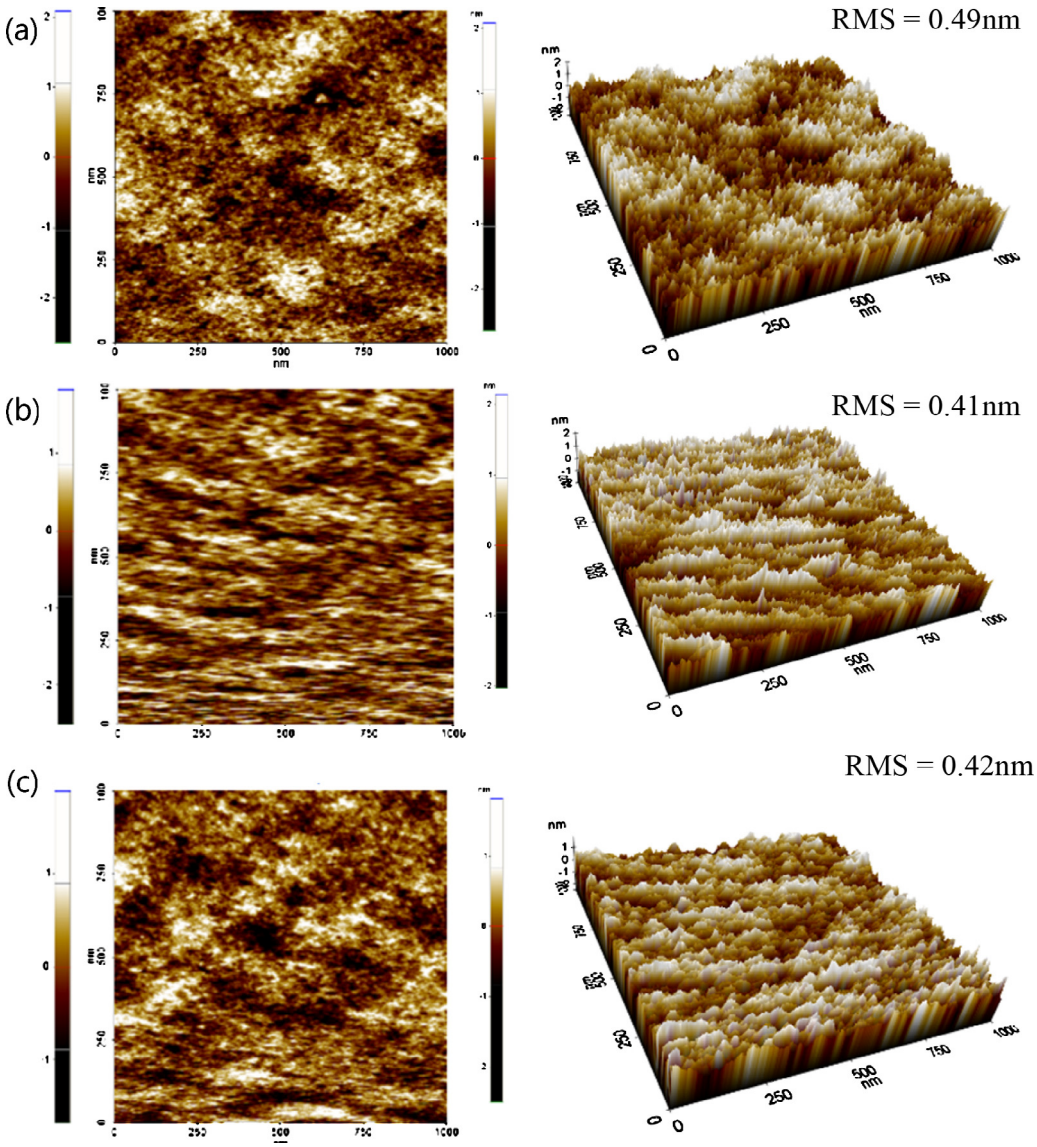

Fig. 6. Topographic AFM images of Polymer:$PC_{71}BM$ (a) P2:$PC_{71}BM$ 1:4 w/w ($1 \times 1\ \mu m^2$), (b) P3:$PC_{71}BM$ 1:4 w/w ($1 \times 1\ \mu m^2$), and (c) P4:$PC_{71}BM$ 1:2 w/w ($1 \times 1\ \mu m^2$).

Moreover, both showed more than 1% PCE. In the case of P3, the small domains and unconnected film formation led to low FF (25%) and J_{sc} (1.4 mA/cm^2), leading to a low PCE of only 0.2% (Fig. 5).

Conclusions

In this study, we used anthracene as a donor and benzothiadiazole and benzoxadiazole as acceptors to prepare four polymers (P1–P4) by Suzuki coupling. The replacement of the sulfur containing BT acceptor by the oxygen containing BO acceptor enhanced the electron withdrawing property of the polymers, inducing long-wavelength absorption and smaller band-gaps. Also, the HOMO energies were lowered due to the high oxidation stability of BO, leading to a consequent improvement in V_{oc}. Polymers P2 and P4, which contain oxygen (BO), showed good charge separation, transportation, and high open-circuit voltages. Consequently, BO-containing polymers showed good efficiency when applied as an active layer in conventional PV cells. Moreover, high PCE values were obtained; namely, 1.2% efficiency with a P2:$PC_{71}BM$ blend (1:4, 0.5 wt%).

Experimental

Instruments and characterization

Unless otherwise specified, all the reactions were carried out under nitrogen atmosphere. Solvents were dried by standard procedures. All column chromatography was performed with the use of silica gel (230–400 mesh, Merck) as the stationary phase. ^1H NMR spectra were performed in a Bruker ARX 400 spectrometer using solutions in $CDCl_3$ and chemical were recorded in ppm units with TMS as the internal standard. The elemental analyses were measured with EA1112 using a CE Instrument. Electronic absorption spectra were measured in chloroform using a HP Agilent 8453 UV–vis spectrophotometer. The cyclic voltammetric waves were produced using a Zahner IM6eX electrochemical workstation with a 0.1 M acetonitrile (substituted with nitrogen for 20 min) solution containing tetrabutyl ammonium hexafluorophosphate (Bu_4NPF_6) as the electrolyte at a constant scan rate of 50 mV/s. ITO, a Pt wire, and silver/silver chloride [Ag in 0.1 M KCl] were used as the working, counter, and reference electrodes, respectively. The electrochemical potential was calibrated against

Fc/Fc^+. The HOMO levels of the polymers were determined using the oxidation onset value. Onset potentials are values obtained from the intersection of the two tangents drawn at the rising current and the baseline changing current of the CV curves. TGA measurements were performed on NETZSCH TG 209 F3 thermogravimetric analyzer. All GPC analyses were made using Chloroform as eluent and polystyrene standard as reference. Topographic images of the active layers were obtained through atomic force microscopy (AFM) in tapping mode under ambient conditions using a XE-100 instrument. All of the GPC analyses were performed using $CHCl_3$ as an eluent and a polystyrene standard as a reference. X-ray diffraction (XRD) patterns were obtained using a SmartLab 3 kW (40 kV 30 mA, Cu target, wavelength: 1.541871 Å) instrument from Rigaku, Japan. Topographic images of the active layers were obtained through atomic force microscopy (AFM) in tapping mode under ambient conditions using an XE-100 instrument. Theoretical analyses were performed using density functional theory (DFT), as approximated by the B3 LYP functional and employing the 6-31G* basis set in Gaussian09. The current density–voltage (*J–V*) curves of the photovoltaic devices were measured using a computer-controlled Keithley 2400 source measurement unit (SMU) that was equipped with a Class A Oriel solar simulator under an illumination of AM 1.5G (100 mW/cm^2). Topographic images of the active layers were obtained through atomic force microscopy (AFM) in tapping mode under ambient conditions using an XE-100 instrument.

Fabrication and characterization of polymer solar cells

All the BHJ photovoltaics (PV) cells were prepared using the following device fabrication procedure. Indium tin oxide (ITO) glass (10 X/sq, Samsung corning) was sequentially sonicated in detergent (Alconox in deionized water, 10%), acetone, isopropyl alcohol, and deionized water for a period of 20 min. The moisture was thoroughly removed with a N_2 gas flow. To ensure the complete removal of the remaining water, the ITO glass was heated on a hot plate for 10 min at 100 °C. For the hydrophilic treatment of the ITO glass surface, the glass was cleaned for 10 min in a UVO cleaner, and poly(3,4-ethylene-dioxythiophene):poly(styrene-sulfonate) (PEDOT:PSS, Baytron P 4083 Bayer AG) was passed through a 0.45-μm filter before being deposited onto the ITO glass to produce a 50-nm-thick layer by spin-coating at 4000 rpm. The coated glass was then dried at 120 °C for 20 min inside a glove box. Composite solutions of the polymer and $PC_{71}BM$ were prepared using *o*-dichlorobenzene (*o*-DCB). The solutions were filtered through a 0.45-μm polytetrafluoroethylene (PTFE) filter and then spin-coated (1000–4000 rpm, 30 s) on top of the PEDOT:PSS layer. The device fabrication was completed by depositing thin layers of BaF_2 (2 nm), Ba (2 nm), and Al (100 nm) at pressures of less than 10^{-6} Torr.

The active area of the device was 0.04 cm^2. Finally, the cell was encapsulated using a UV-curing glue (Nagase, Japan). All devices were fabricated with the following structure: ITO glass/PEDOT:PSS/polymer:$PC_{71}BM$/BaF_2/Ba/Al. The output photocurrent was adjusted to match the photocurrent of the Si reference cell to obtain a power density of 100 mW/cm^2. After encapsulation, all devices were operated under ambient atmosphere at 25 °C.

Materials

All reagents were purchased from Aldrich, Acros, or TCI. All of the chemicals were used without further purification. Toluene and tetrahydrofuran (THF) were distilled from benzophenone ketyl and sodium. 5,6-Bis(octyloxy)-benzo-2,1,3-thiadiazole and 5,6-bis(octyloxy)-benzo-2,1,3-oxadiazole were synthesized according to previous procedures [20,24].

2,6-Bis(4,4,5,5-tetramethyl-1,3,2-dioxaborolan-2-yl)anthracene (D1)

2,6-Dibromoanthracene(2.00 g, 6.46 mmol) 1, bis(pinacolato)-diboron (4.16 g, 16.16 mmol), $PdCl_2$ (dppf) (0.164 g, 26.38 mmol), and potassium acetate (KOAc) (2.5 g, 26.38 mmol) were added in Schlenk flask and kept under vacuum for 10 min. Under an argon flow anhydrous 1,4-dioxane (40 mL) was added to above mixture and the mixture was stirred at room temperature for 30 min before it was heated at 80 °C and stirred for 20 h. The resulting mixture was quenched by adding water and extracted with ethyl acetate (100 mL). The combined organic layers were washed with brine, dried over Na_2SO_4, and filtered. After removing the solvent, a dark red solid was obtained, which was purified by silica gel chromatography by using 5% ethyl acetate in hexane as eluent to give the title compound as yellow solid (2.0 g, 71%). ^1H NMR (400 MHz, $CDCl_3$): δ 8.55 (s, 2*H*), 8.44 (s, 2*H*), 8.01 (dd, 2*H*), 7.76 (dd, 2*H*), 1.39 (s, 24*H*).

2,6-Dibromo-9,10-bis(2-ethylhexyloxy)-9,10-dihyroanthracene (1)

2,6-Dibromo-9,10-anthraquinone (2.0 g, 5.4 mmol), tetrabutylammonium bromide (1.6 g, 4.9 mmol), $Na_2S_2O_4$ (1.9 g, 11 mmol), and water (50 mL) were added under nitrogen. The mixture was stirred for 10 min, and CH_2Cl_2 (60 mL) was added. When the solution turned to a green color, 20% NaOH (aq) was added and stirred for 2 h. To this solution was added 2-ethylhexyl bromide (8.8 g, 54 mmol), and the mixture was stirred for 8 h. The product was purified on a silica column using hexane/CH_2Cl_2 (5:1) as the eluent. Yield: 2.0 g (70%). Mp: 127–129 °C. ^1H NMR (400 MHz, $CDCl_3$): δ 8.36 (d, 2*H*), 8.21 (s, 2*H*), 7.64 (dd, 2*H*), 4.11 (t, 4*H*), 1.69 (m, 4*H*), 1.28 (m, 12*H*), 0.91 (t, 6*H*).

2,2′-(9,10-Bis(2-ethylhexyloxy)-9,10-dihydroanthracene-2,6-diyl)bis(4,4,5,5-tetramethyl-1,3,2-dioxaborolane) (D2)

Bu-Li was added a 2,6-dibromo-9,10-bis(2-ethylhexyloxy)-9,10-dihyroanthracene (1.4 g, 2.4 mmol) in THF at −78 °C. After string 1 h, 2-Isopropoxy-4,4,5,5-tetramethyl-1,3,2-dioxaborolane was added in solution. The reaction mixture was warmed to room temperature and stirred for 24 h. The resulting mixture was quenched by adding water and extracted with methylene chloride. The combined organic layers were washed with brine, dried over Na_2SO_4, and filtered. After removing the solvent, which was purified by silica gel chromatography by using hexane/CH_2Cl_2 (4:1) as eluent to give the title compound as yellow solid (1.23 g, 76%). ^1H NMR (400 MHz, $CDCl_3$): δ 8.55 (s, 2*H*), 8.44 (s, 2*H*), 8.01 (dd, 2*H*), 7.76 (dd, 2*H*), 1.39 (s, 24*H*).

4,7-Dibromo-5,6-bis(octyloxy)-benzo-2,1,3-thiadiazole (2a)

A solution of bromine (0.15 mL, 0.48 g, 3.0 mmol) in 5 mL 40% hydrobromic acid was added dropwise to the mixture of 5,6-bis(octyloxy)-benzo-2,1,3-thiadiazole (0.39 g, 1.0 mmol) in 10 mL 40% hydrobromic acid at room temperature. After being refluxed at 120 °C for 6 h, the excess bromine was neutralized completely by saturated $NaHSO_3$ solution. Then, the reaction mixture was extracted by CH_2Cl_2 (3 × 50 mL) and the combined organic layers were dried over anhydrous Na_2SO_4. The organic solvent was evaporated under reduced pressure and, the crude product was purified by silica column chromatography eluting with petroleum ether/ethyl acetate (v:v, 20:1) to afford compound 6 as a white solid (0.50 g, 90%). M.p.: 44–45 °C; ^1H NMR (400 MHz, $CDCl_3$, ppm): δ 4.16 (t, J = 6.6 Hz, 4*H*), 1.92–1.85 (m, 4*H*), 1.58–1.50 (m, 4*H*), 1.41–1.30 (m, 16*H*), 0.90 (t, J = 6.6 Hz, 6*H*).

5,6-Bis(octyloxy)-4,7-di(thiophene-2-yl)-benzo-2,1,3-thiadiazole (3a)

A solution of *n*-BuLi (2.5 M in hexane, 3.2 mL, 8.0 mmol) was added dropwise to the mixture of thiophene (0.48 mL, 0.50 g, 6.0 mmol) in 30 mL dry THF under nitrogen atmosphere at −78 °C

and the reaction mixture was stirred at that temperature for 1 h. Then, tributylchlorostannane (2.2 mL, 2.6 g, 8.0 mmol) was added to the mixture in one portion. After being stirred at room temperature overnight, the resulting mixture was poured into water (50 mL), and the organic layer was separated. The aqueous layer was extracted with ethyl ether (3 × 30 mL), and the combined organic layers were dried over anhydrous Na_2SO_4. The crude product was obtained by removing organic solvent under reduced pressure and purified by silica column chromatography eluting with petroleum/triethylamine (v:v, 20:1) to afford 2-tri(*n*-butyl)stannylthiophene as a light yellow oil. The 2-tri(*n*-butyl)stannylthiophene (freshly prepared, about 6.0 mmol), and compound 6 (1.0 g, 1.8 mmol) were dissolved in 30 mL dry THF. After being degassed with nitrogen, to the mixture was added $Pd(PPh_3)_2Cl_2$ (70 mg, 0.1 mmol) and the resulting mixture was heated at 70 °C for 40 h. Then, the organic solvent was evaporated under reduced pressure, and the crude product was purified by silica column chromatography eluting with petroleum ether/CH_2Cl_2 (v:v, 4:1) to afford compound 7 as an orange oil (0.96 g, 96%). ^{1}H NMR (400 MHz, $CDCl_3$, ppm): δ 8.43 (dd, J_a = 3.8 Hz, J_b = 1.0 Hz, 2*H*), 7.52 (dd, *J* = 5.0 Hz, *J* = 1.0 Hz, 2*H*), 7.22 (dd, J_a = 5.0 Hz, *J* = 3.8 Hz, 2*H*), 4.07 (t, *J* = 7.0 Hz, 4*H*), 1.94–1.85 (m, 4*H*), 1.58–1.30 (m, 20*H*), 0.90 (t, *J* = 6.6 Hz, 6*H*).

4,7-Bis(5-bromothiophene-2-yl)-5,6-bis(octyloxy)-benzo-2,1,3-thiadiazole (A1)

The mixture of compound 6 (0.96 g, 1.7 mmol) and *N*-Bromosuccinimide (NBS, 0.73 g, 4.1 mmol) in 30 mL $CHCl_3$ was stirred for 24 h in dark. Then, the organic solvent was evaporated under reduced pressure, and the crude product was purified by silica column chromatography eluting with petroleum ether/CH_2Cl_2 (v:v, 10:1) to afford compound A as an orange–red solid (1.1 g, 92%). M.p.: 74–76 °C; ^{1}H NMR (400 MHz, $CDCl_3$, ppm): δ 8.33 (d, *J* = 4.0 Hz, 2*H*), 7.13 (d, *J* = 4.0 Hz, 2*H*), 4.10 (t, *J* = 7.2 Hz, 4*H*), 1.98–1.90 (m, 4*H*), 1.47–1.25 (m, 20*H*), 0.90 (t, *J* = 6.6 Hz, 6*H*).

4,7-Dibromo-5,6-bis(octyloxy)benzo[c][1,2,5]oxadiazole (2b)

AcOH (10 mL) and Br_2 (0.850 mL, 16.6 mmol) were added sequentially to a solution of 5,6-bis(octyloxy)benzo[*c*][1,2,5]oxadiazole (1.50 g, 4.00 mmol) in CH_2Cl_2 (80 mL). The resulting mixture was stirred in the dark for 3 days at room temperature and then poured into aqueous NaOH solution (10 g in 200 mL). The aqueous phase was extracted with CH_2Cl_2; the combined organic extracts were washed with brine and concentrated under reduced pressure to afford a crude solid that was purified through column chromatography [SiO_2, hexane/CH_2Cl_2, 9:1 (v/v)]. A white solid (2.2 g, 79%). ^{1}H NMR (400 MHz, $CDCl_3$): δ 4.13 (t, *J* = 9 Hz, 4*H*), 1.89–1.80 (m, 4*H*), 1.53–1.29 (m, 20*H*), 0.88 (t, *J* = 6.6 Hz, 6*H*).

5,6-Bis(octyloxy)-4,7-di(thiophen-2-yl)benzo[c][1,2,5]oxadiazole (3b)

4,7-Dibromo-5,6-bis(octyloxy)benzofurazan (2.06 g, 4.1 mmol), tributyl(thiophen-2-yl)stannane (4.6 g, 12.3 mmol) and $Pd(PPh_3)_2Cl_2$ (287.7 mg, 0.41 mmol) were dissolved in 41 ml THF and refluxed overnight. THF was evaporated, and the resulting mixture was purified by column chromatography in hexane: DCM = 10: 1 as mixed eluent, and yielded 2.0 g of the target compound as a yellow solid. ^{1}H NMR (400 MHz, $CDCl_3$, d): 8.46 (dd, *J* = 3.84 Hz, 2*H*, ArH), 7.50 (dd, *J* = 5.16 Hz, 2*H*, ArH), 7.22 (t, 2*H*, ArH), 4.15 (t, 4*H*, CH_2), 1.98 (m, 4*H*, CH_2), 1.47–1.30 (br, 20*H*, CH_2), 0.90 (t, 6*H*, CH_3).

4,7-Bis(5-bromothiophen-2-yl)-5,6-bis(octyloxy)benzo[c][1,2,5]oxadiazole (A2)

To a solution of 4,7-di(thiophen-2-yl)-5,6-bis(octyloxy) benzofurazan (2 g, 3.7 mmol) in 42 ml chloroform and 42 ml AcOH in the absence of light, NBS (1.45 g, 8.14 mmol) was added in small portions. Then, the reaction continued for 48 h. Water was added and extracted by DCM three times, washed by NaCl aqueous solution and water, respectively, and dried over Na_2SO_4. The solvent was removed by evaporation, and the resulting product was purified by column chromatography in petroleum ether as eluent, and yielded 2.2 g of the target compound as an orange solid. ^{1}H NMR (400 MHz, $CDCl_3$, d): 8.24(d, *J* = 4.14 Hz, 2*H*, ArH), 7.17(d, *J* = 4.14 Hz, 2*H*, ArH), 4.15(t, 4*H*, CH_2), 1.99(m, 4*H*, CH_2), 1.55–1.31(br, 20*H*, CH_2), 0.91(t, 6*H*, CH_3).

Polymerization

Poly[2,6-anthracene-alt-*4,7-bis(thiophen-2-yl)-5,6-bis(octyloxy)benzo[c][1,2,5]thiadiazole], P1*

D1 (0.172 g, 0.4 mmol), A1 (0.286 g, 0.4 mmol), $Pd(PPh_3)_4$(0) (0.015 g, 0.016 mmol), tris(dibenzylideneacetone)dipalladium(0) (14.65 mg, 0.016 mmol), tri-(*o*-toly)phosphine (11.5 mg, 0.0378 mmol) and Aliquat336, were placed in a Schlenk tube, purged with three nitrogen/vacuum cycles, and under a nitrogen atmosphere, added 2 M degassed aqueous K_2CO_3 (4 mL), and dry toluene (15 mL). The mixture heated to 90 °C for 48 h. After the polymerization was completed, the polymer was end-capped with phenylboronic acid and bromothiophene. After reaction quenching, the entire mixture was poured into methanol. The precipitate was filtered off and purified with a soxhlet extraction in the following order: methanol, acetone, and chloroform. The polymer was recovered from the chloroform fraction and precipitated into methanol. The final product was obtained after drying in vacuum. Dark purple solid (0.085 g, 29%). ^{1}H NMR: δ 7.59–8.53 (m, 12*H*), 4.16 (d, 4*H*), 1.30–1.97 (m, 24*H*), 0.75 (t, 6*H*). Anal. calcd. for $C_{44}H_{48}N_2O_2S_3$ C, 72.09; H, 6.60; N, 3.82; O, 4.37; S, 13.12; found C 71.47, H 7.40, N 2.99, O 5.44, S 9.73.

P2, P3 and P4 were synthesized according to the same procedure. ^{1}H NMR and elemental analysis for the polymers are presented.

Poly[2,6-anthracene-alt-*4,7-bis(thiophen-2-yl)-5,6-bis(octyloxy)benzo[c][1,2,5] oxadiazole], P2*

Dark purple solid (0.21 g, 59%). ^{1}H NMR: δ 7.29–8.36 (m, 12*H*), 4.24 (d, 4*H*), 1.20–2.10 (m, 24*H*), 0.82 (t, 6*H*). Anal. calcd. for $C_{44}H_{48}N_2O_3S_2$ C, 73.71; H, 6.75; N, 3.91; O, 6.69; S, 8.94; found C 76.67, H 9.30, N 2.49, O 5.40, S 5.45.

Poly[9,10-bis(2-ethylhexyloxy)anthracene-alt-*4,7-bis(thiophen-2-yl)-5,6-bis(octyloxy)benzo [c][1,2,5]thiadiazole], P3*

Dark purple solid (0.32 g, 82%). ^{1}H NMR: δ 7.31–8.63 (m, 10*H*), 4.15 (d, 4*H*), 1.06–2.04 (m, 24*H*), 0.97 (t, 6*H*). Anal. calcd. for $C_{62}H_{84}N_2O_4S_3$ C, 73.18; H, 8.32; N, 2.75; O, 6.29; S, 9.45; found C 72.68, H 7.20, N 2.96, O 8.38, S 8.60.

Poly[9,10-bis(2-ethylhexyloxy)anthracene-alt-*4,7-bis(thiophen-2-yl)-5,6-bis(octyloxy)benzo [c][1,2,5]oxadiazole], P4*

Dark purple solid (0.23 g, 59%). ^{1}H NMR: δ 7.24–8.61 (m, 10*H*), 4.15 (d, 4*H*), 0.96–2.08 (m, 24*H*), 0.88 (t, 6*H*). Anal. calcd. for $C_{62}H_{84}N_2O_5S_2$ C, 74.36; H, 8.45; N, 2.80; O, 7.99; S, 6.40; found C 72.31, H 7.89, N 2.91, O 9.55, S 6.43.

Competing interest

The authors declare no competing financial interest.

Acknowledgments

This paper was supported by Konkuk University in 2012.

Appendix A. Supplementary data

Supplementary data associated with this article can be found, in the online version, at doi:10.1016/j.jiec.2015.10.010.

References

[1] Min Hee Choi, Kwan Wook Song, Soo Won Heo, Yong Woon Han, Doo Kyung Moon, J. Ind. Eng. Chem. 26 (2015) 173–181.
[2] Kwan Wook Song, Tae Ho Lee, Eui Jin Ko, Kyung Hun Back, Doo Kyung Moon, Polym. Chem. 52 (2014) 1028–1036.
[3] Jin-Mun Yun, Chan-Hee Jung, Yong-Jin Noh, Ye-Jin Jeon, Seok-Soon Kim, Dong-Yu Kim, Seok-In Na, J. Ind. Eng. Chem. 21 (2015) 877–883.
[4] Tae-Woon Kang, Yong-Jin Noh, Seok-Soon Kim, Han-Ik Joh, Seok-In Na, J. Ind. Eng. Chem. 24 (2015) 206–210.
[5] Christoph J. Brabec, Srinivas Gowrisanker, Jonathan J.M. Halls, Darin Laird, Shijun Jia, Shawn P. Williams, Adv. Mater. 22 (2010) 3839–3856.
[6] G. Yu, J. Gao, J.C. Hummelen, F. Wudl, A.J. Heeger, Science 270 (1995) 1789–1791.
[7] Ho Jun Song, Munju Goh, Kyung Ho Choi, Sangkug Lee, Doo Kyung Moon, Gyo Jic Shin, J. Ind. Eng. Chem. 23 (2015) 338–343.
[8] Huaxing Zhou, Liqiang Yang, Wei You, Macromolecules 45 (2012) 607–632.
[9] Nuha Ahmed Wazzan, J. Ind. Eng. Chem. 26 (2015) 291–308.
[10] Kwan Wook Song, Min Hee Choi, Ho Jun Song, Soo Won Heo, Jang Yong Lee, Doo Kyung Moon, Sol. Energy Mater. Sol. Cells 120 (2014) 303–309.
[11] Iain Meager, Raja Shahid Ashraf, Sonya Mollinger, Bob C. Schroeder, Hugo Bronstein, Daniel Beatrup, Michelle S. Vezie, Thomas Kirchartz, Alberto Salleo, Jenny Nelson, Iain McCulloch, J. Am. Chem. Soc. 135 (2013) 11537–11540.
[12] Jacobus J. van Franeker, Gaël H.L. Heintges, Charley Schaefer, Giuseppe Portale, Weiwei Li, Martijn M. Wienk, Paul van der Schoot, René A.J. Janssen, J. Am. Chem. Soc. 137 (2015) 11783–11794.
[13] Tae In Ryu, Youngwoon Yoon, Ji-Hoon Kim, Do-Hoon Hwang, Min Jae Ko, Doh-Kwon Lee, Jin Young Kim, Honggon Kim, Nam-Gyu Park, BongSoo Kim, Hae Jung Son, Macromolecules 47 (2014) 6270–6280.
[14] Lingcheng Chen, Linquan Huang, Dong Yang, Shuying Ma, Xin Zhou, Jian Zhang, Guoli Tu, Can Li, J. Mater. Chem., A 2 (2014) 2657–2662.
[15] Ram S. Bhatta, Mesfin Tsige, Int. J. Photoenergy 2015 (2015) 7.
[16] Hong Meng, Fangping Sun, Marc B. Goldfinger, Gary D. Jaycox, Zhigang Li, Will J. Marshall, Gregory S. Blackman, J. Am. Chem. Soc. 127 (2005) 2406–2407.
[17] L. Ai, X.H. Ouyang, Q.D. Liu, S.Y. Wang, R.X. Peng, A. Islam, Z.Y. Ge, Dyes Pigm. 115 (2015) 73–80.
[18] Chunchen Liu, Wanzhu Cai, Xing Guan, Chunhui Duan, Qifan Xue, Lei Ying, Fei Huang, Yong Cao, Polym. Chem. 4 (2013) 3949.
[19] Zbyslaw R. Owczarczyk, Wade A. Braunecker, Andres Garcia, Ross Larsen, Alexandre M. Nardes, Nikos Kopidakis, David S. Ginley, Dana C. Olson, Macromolecules 46 (2013) 1350–1360.
[20] Ping Ding, Cheng-Che Chu, Yingping Zou, Dequan Xiao, Chunyue Pan, Chain-Shu Hsu, J. Appl. Polym. Sci. 123 (2012) 99–107.
[21] Takeshi Yasuda, Yuki Shinohara, Takaaki Matsuda, Liyuan Hana, Tsutomu Ishi-I, J. Mater. Chem. 22 (2012) 2539–2544.
[22] Andrew J. Pearson, Darren C. Watters, Hunan Yi, Mohd S. Sarjadi, Luke X. Reynolds, Pier P. Marchisio, James Kingsley, Saif A. Haque, Ahmed Iraqi, David G. Lidzey, RSC Adv. 4 (2014) 43142.
[23] Robert C. Coffin, Christopher M. MacNeill, Eric D. Peterson, Jeremy W. Ward, Jack W. Owen, Claire A. McLellan, Gregory M. Smith, Ronald E. Noftle, Oana D. Jurchescu, David L. Carroll, J. Nanotechnol. 2011 (2011) 10.
[24] Jian-Ming Jiang, Po-An Yang, Tsung-Hsuan Hsieh, Kung-Hwa Wei, Macromolecules 44 (2011) 9155–9163.
[25] Jian-Ming Jiang, Po-An Yang, Hsiu-Cheng Chen, Kung-Hwa Wei, Chem. Commun. 47 (2011) 8877–8879.
[26] Seza Gökera, Gonul Hızalana, Yasemin Arslan Udumd, Levent Toppare, Synth. Met. 191 (2014) 19–27.
[27] Palas Baran Pati, Satyaprasad P. Senanayak, K.S. Narayan, Sanjio S. Zade, ACS Appl. Mater. Interfaces 5 (2013) 12460–12468.
[28] Jian-Ming Jiang, Hsiu-Cheng Chen, His-Kuei Lin, Chia-Ming Yu, Shang-Che Lan, Chin-Ming Liu, Kung-Hwa Wei, Polym. Chem. 4 (2013) 5321.
[29] Jian-Ming Jiang, Po-An Yang, Shang-Che Lan, Chia-Ming Yu, Kung-Hwa Wei, Polymer 54 (2013) 155–161.
[30] Thu Trang Do, Ye Eun Ha, Joo Hyun Kim, Org. Electron. 14 (2013) 2673–2681.
[31] Bo Liu, Xuewen Chen, Yuehui He, Yongfang Li, Xinjun Xu, Lu Xiao, Lidong Li, Yingping Zou, J. Mater. Chem., A 1 (2013) 570–577.
[32] Doo Hun Kim, Ho Jun Song, Soo Won Heo, Kwan Wook Song, Doo Kyung Moon, Sol. Energy Mater. Sol. Cells 120 (2014) 94–101.
[33] Kwan Wook Song, Min hee Choi, Myung hee Han, Doo Kyung Moon, J. Ind. Eng. Chem. 20 (2014) 426–434.
[34] Shiming Zhang, Yunlong Guo, Hongxia Xi, Chong-an Di, Jian Yu, Kai Zheng, Ruigang Liu, Xiaowei Zhan, Yunqi Liu, Thin Solid Films 517 (2009) 2968–2973.
[35] Wouter Vanormelingen, Lesley Pandey, Mark Van der Auweraer, Thierry Verbiest, Guy Koeckelberghs, Macromolecules 43 (2010) 2157–2168.
[36] Jean Bouffard, Timothy M. Swager, Macromolecules 41 (2008) 5559–5562.
[37] Ji-Hoon Kim, Jong Baek Park, Hee Un Kim, In-Nam Kang, Do-Hoon Hwang, Synth. Met. 194 (2014) 88–96.
[38] Xiaochen Wang, Yeping Sun, Song Chen, Xia Guo, Maojie Zhang, Xiaoyu Li, Yongfang Li, Haiqiao Wang, Macromolecules 45 (2012) 1208–1216.
[39] Shamsa Bibi, Jingping Zhang, Phys. Chem. Chem. Phys. 17 (2015) 7986–7999.
[40] Jian-Ming Jiang, Putikam Raghunath, Hsi-Kuei Lin, Yu-Che Lin, M.C. Lin, Kung-Hwa Wei, Macromolecules 47 (2014) 7070–7080.
[41] Soo Won Heo, Kyeong Hun Baek, Ho Jun Song, Tae Ho Lee, Doo Kyung Moon, Macromol. Mater. Eng. 299 (2014) 353–360.
[42] A. Maoucha, F. Djeffal, J. Comput. Electron. 11 (2012) 336–343.
[43] Hyojin Kang, Su Yeon An, Bright Walker, Seyeong Song, Taehyo Kim, Jin Young Kim, Changduk Yang, J. Mater. Chem., A 3 (2015) 9899–9908.
[44] Stephanie R. Dupont, Eszter Voroshazi, Dennis Nordlund, Reinhold H. Dauskardt, Sol. Energy Mater. Sol. Cells 132 (2015) 443–449.
[45] Haiyang Wang, Yaozhuo Xu, Xinhong Yu, Rubo Xing, Jiangang Liu, Yanchun Han, Polymers 5 (2013) 1272–1324.